IEEE Access
Multidisciplinary ⋮ Rapid Review ⋮ Open Access Journal

Received 25 April 2024, accepted 6 May 2024, date of publication 13 May 2024, date of current version 28 May 2024.

Digital Object Identifier 10.1109/ACCESS.2024.3400671

RESEARCH ARTICLE

A Low-Profile Shared Aperture Antenna for FR1 and FR2 5G Frequency Bands

MARCO SIMONE[1,2], (Member, IEEE), SANTI CONCETTO PAVONE[1,2], (Senior Member, IEEE), MATTEO BRUNO LODI[3,4], (Member, IEEE), NICOLA CURRELI[5], (Member, IEEE), GIACOMO MUNTONI[3,4], (Member, IEEE), ALESSANDRO FANTI[3,4], (Senior Member, IEEE), GINO SORBELLO[1,2], (Member, IEEE), AND GIUSEPPE MAZZARELLA[3,4], (Senior Member, IEEE)

[1]Department of Electrical, Electronics, and Computer Engineering (DIEEI), University of Catania, 95123 Catania, Italy
[2]University of Catania Research Unit, National Inter-University Consortium for Telecommunications (CNIT), 43124 Parma, Italy
[3]Department of Electrical and Computer Engineering, University of Cagliari, 09123 Cagliari, Italy
[4]University of Cagliari Research Unit, National Inter-University Consortium for Telecommunications (CNIT), 09123 Cagliari, Italy
[5]Functional Nanosystems Group, Istituto Italiano di Tecnologia (IIT), 16163 Genoa, Italy

Corresponding author: Alessandro Fanti (alessandro.fanti@unica.it)

This work was partially supported in part by the Sardegna Ricerche-Regione Autonoma della Sardegna- Programma Regionale di Sviluppo 2020–2024; Strategia 2—Identità economica; Progetto 2.1– Ricerca e innovazione tecnologica; Research and Development Program ICT (Information and Communication Technologies); through ''SAURON5G'' contract under Grant CUP F23D23000170002. Moreover, this work was partially supported by the European Union under the Italian National Recovery and Resilience Plan (NRRP) of NextGenerationEU, partnership on ''Telecommunications of the Future'' (PE0000001 - program ''RESTART'', Structural Project DREAMS). Santi C. Pavone would like to thank the project PIA.CE.RI., Linea di intervento 3 ''Starting Grant'', granted by the University of Catania, Italy. This work has been developed within the framework of the project eINS-Ecosystem of Innovation for Next Generation Sardinia (cod. ECS 00000038) funded by the Italian Ministry for Research and Education (MUR) under the National Recovery and Resilience Plan (PNRR) - MISSION 4 COMPONENT 2, ''From research to business'' INVESTMENT 1.5, ''Creation and strengthening of Ecosystems of innovation'' and construction of ''Territorial R&D Leaders'').

ABSTRACT Shared-aperture antennas are attracting a wide interest in last of years, due to their inherent compactness and low-profile layout. More specifically, in this work a shared-aperture antenna for FR1 and FR2 frequency bands is proposed. The difference in size between the radiating elements operating the two frequency bands can be exploited to embed different antennas in the same area. A 4×4 patch array for FR2 is embedded inside a FR1 shaped patch antenna. The antenna system is designed by preserving a low-profile architecture suitable for planar technology. The performance of the antenna system are evaluated for both the bands achieving a 10-dB bandwidth equal to 0.14 GHz (3.8 %) for FR1 and to 2.32 GHz (8.6 %) for FR2. In FR2, a $\pm 30°$ steering capability along the H plane is shown.

INDEX TERMS Antenna, shared aperture, 5G, dual band, FR1, FR2, patch, beam steering.

I. INTRODUCTION

The new generation of communication technologies is going to deeply revolutionize telecommunications and their impact in several fields of industry and daily life. Indeed, the wide frequency bands available in mm-wave frequency range and the low latencies will make possible new applications as high-resolution streaming [1], large IoT [2], remote surgery [3], or self-driving vehicles [4].

The associate editor coordinating the review of this manuscript and approving it for publication was Davide Ramaccia.

5G technologies are intended to offer communication services over different frequency ranges. The Frequency Range 1 (FR1), which includes the sub-6 GHz frequency bands, covers the spectrum from 410 MHz to 7125 MHz, whereas the Frequency Range 2 (FR2) includes the frequency band from 24.25 GHz to 71 GHz [5]. The low frequencies around 3.7 GHz are employed as standard for mobile communications (RESOLUTION 246 (WRC-19), [5]), whereas the mm-wave will be dedicated to high-performance services or to guarantee desired connections in crowded environments, as cinemas, stadiums or shopping

TABLE 1. State of the art of shared aperture antennas for FR1-FR2 5G.

Ref.	Year	FR1				FR2					Multi-layer	Profile Height [mm]	Size [mm^2]
		Antenna Element	Array ele-ments	BW [GHz]	Gain [dBi]	Antenna Element	Array ele-ments	BW [GHz]	Gain [dBi]	BS [°]			
[17]	2021	Dual-pol. cross-dipole	16	2.76–4.2 (41.38%)	9	Ground-backed Printed dipole	80	24.9–27.8 (11.01%)	9.7	NA	yes	3.11	400×400
[18]	2021	ME dipole	2×2	2.35–3.93 (50.32%)	10.67	Horn ME dipole fed	2×2	24–33.91 (34.23%)	14.85	±20°	yes	>10	120×120
[19]	2022	Metasurface patch	-	3.2-3.45 (7.52%)	6.2	Patch fed Luneburg lens	-	25.5-29.5 (14.55%)	19.3	±28°	yes	>10	>100
[20]	2020	Metasurface-based antenna	3×3	3.2–4.05 (23.45 %)	10.44	FPRA	18×18	26.8–29.55 (9.76 %)	14.6	NA	yes	7.34	92×92
[21]	2023	Patch-fed PRS resonant cavity	-	3.45-3.58 (3.7%)	4.85	Stacked patch	8×8	24.5-27 (9.71%)	22.5	±45°	yes	24	100×100
[22]	2024	ME dipole	-	1.61-2.45 (41.3%)	10.2	Horn	-	20-36.4 (58.2%)	17.4	NA	no	32.94	150×150
[23]	2020	Dipole-fed reflector	1×2 dipole	3.38–3.92 (14.79%)	13	Circular horn-fed reflector	-	24.9–40 (46.5%)	30.8	NA	no	118.7	216

BW = Bandwidth, BS = Beam Steering,
ME = magnetoelectric, PRS = Partially reflective surface, FPRA = Fabri-Perot resonator antenna,
NA = Not Available

centres [6], [7]. This increases the number of Access Points which needs to be installed in the environment, especially for the mm-wave frequency bands, due to signal attenuation in air which is a relevant issue at these frequency, and to the non-line-of-sight (NLOS) propagation. Therefore, the need of a large number of installations has an environmental impact which becomes more important with respect to former communication technology generations. For these reasons, a solution which reduces the number of installations leads to different advantages in terms of space saving and energy consumption. This is a notable advantage also when the antenna system is embedded in a mobile device, where a radiating element servicing multiple frequency bands increases the system integration, and allows to save space in the reduced size of the board which contains all the electronics of a smartphone. The demand of compact antenna systems which can support microwave (MW) and millimeter-wave (MMW) frequency bands simultaneously for wireless terminals, such as mobiles, vehicles or drones, reducing the number of antennas and the manufacturing costs, pushes the development of FR1-FR2 dual-band antennas for the emerging 5G technology.

The concept of arranging different antennas operating in different frequency bands in the same aperture is called shared-aperture antenna [8], [9], [10], [11], [12], [13], [14], [15], [16]. In the last years, this solution is attracting a growing interest, by combining antennas operating in different bands, from the S to the V [8]. The investigation carried on by the scientific community has involved a large set of antenna technologies, e.g. a Ka-band reflectarray accommodated in the same aperture of a S-band patch array for nanosatellite platforms [9]. Apart from this first example, commonly share aperture multiband antennas exploit multilayer layouts to arrange the antennas geometry. In [10] patch-dipole antenna elements in Ku and microstrip patch antenna elements in Ka are combined in a 4 layer laminates substrate. In [11], a multilayer structure exploits a continuous transverse stub antenna in the top radiating layers, operating in Ku and K band, and a non-uniform slow wave structure for the feeding network. In [12], a multilayer printed antenna system combined an array of driven patch with an overlying layer of parasite patches to cover X and Ku bands with a dual polarized operation. Parasitic elements on the top layer are exploited also in [13] to suppress the side lobe levels caused by the array spacing, in a Ku/Ka band antenna array. On the other hand, only-metal antennas (e.g. cavity backed waveguide slot antenna arrays) have been recently proposed to overcome the issues due to the losses in high-Ku and higher frequencies, as in SatCom applications [14], [15]. As a matter of fact, shared aperture antennas prove useful in applications where space occupancy is a critical issue, which is typical in satellites [16].

TABLE 2. State of the art of planar low profile shared aperture antennas for FR1-FR2 5G.

Ref.	Year	FR1				FR2					Multi-layer	Profile Height [mm]	Size [mm^2]
		Antenna Element	Array ele-ments	BW [GHz]	Gain [dBi]	Antenna Element	Array ele-ments	BW [GHz]	Gain [dBi]	BS [°]			
[24]	2022	Slot	-	3.48-3.62 (3.94%)	2.5	Slot	4×1	26.52–30.14 (12.78 %)	9.8	±30°	no	3.4	147×72
[25]	2022	Capacity coupled element	-	1.70–5.30 (*[1])	5	Patch with parasite elements	3×1	27.5–28.35 (3.04%)	7.9	±45°	yes	1.12	34 × 8
[26]	2022	Perforated patch antenna	-	3.38–3.64 (7.4%)	6.9	Patch	4×2	26.4–29.8 (12.1%)	14.6	±30°	yes	3.42	34.26× 22.27
[27]	2020	Slot-fed dipole	-	3.6	4	Tapered slot	2	28	8	±60°	no	0.324	75×25
[28]	2024	Annular patch antenna	-	3.4-3.6 (5.71%)	10.65	SIW slot ar-ray	4×4	26.5-29.5 (10.71%)	18.5	NA	no	1.1	140×140
This work		Perforated Patch Antenna	-	3.63-3.76 (3.5 %)	7	Patch	4×4	26.32-27.44 (4.17%)	18.54	±30°	no	0.857	80×80

BW = Bandwidth, BS = Beam Steering, (*[1]) (6dB BW)

The works [8], [9], [10], [11], [12], [13], [14], [15], [16] highlight a relevant interest in the development of multi-band antenna systems in these years, for its advantages in terms of space saving and embedding. This interest embraces also antenna systems which combine different operating bands of the 5G. Indeed, the development of 5G multi-band antennas is rising in the last years, and it is not deeply investigated yet. In [17], different dipole-shaped antennas are combined in a base station to cover the 0.8, 3.7 and 26.5 GHz frequency ranges, in a layout 40 × 40 cm^2 large based on multilayer made of FR-4 and Rogers RO3003. In [18], a dual-band dual-polarized magnetoelectric dipole antenna for the FR1 and FR2 frequency bands is proposed. In [19], a metasurface antenna is integrated with a slimmed flat Luneburg lens, to obtain the desired gain at mm-wave with a single patch antenna. A metasurface is employed also in [20], where it acts as antenna in S-band and as a partially reflective surface (PRS) in Ka. In [21], the mm-wave array works as PRS of a sub-6 GHz resonant cavity antenna. A FR2 horn embedded in the layout of a shaped magnetoelectric dipole has been proposed in [22]. Also, antennas involving reflectors [23] have been proposed. A summary of these works is shown in Table 1.

It appears that several kinds of radiating elements have been exploited and combined to design different models of shared-aperture antennas, and commonly multilayer substrates or, in any case, bulky structures have been chosen, especially to obtain a FR2 bandwidth (BW) larger than 1 GHz. Antennas as [18], [22], [23] provide a very wide bandwith at the price of bulky geometries. Nevertheless, the choice of multilayer (or bulky-3D) geometries, increases the design complexity and, therefore, the manufacturing costs, which is a disadvantage in terms of antenna potential employments in the commercial sphere. Following this purpose, in Table 2 other works which are oriented to low-profile solutions (and with an easier manufacturing process) are listed, e.g. intended for mobile terminals [24], [25]. In [26] a 2 × 2.28 GHz patch array is integrated inside a 3.5 GHz perforated patch antenna. In [27], a tapered slot is used both to feed a 3.6 GHz dipole antenna and as end-fire antenna at 28 GHz. In [28], a mm-wave siw slot array is placed inside an annular patch antenna.

Among the aforementioned works, [25], [26], [28] involve multilayered structures, whereas [24], [27] are single layers which exploit slots as radiating elements for both the frequency ranges. In addition, [24] and [27] involve coaxial connectors to feed the antenna array. In the tables, we did not involve the coaxial feed in the profile height evaluation, similarly as we do to evaluate our design. In this work, a simple solution which embeds both a 3.7 GHz antenna and a 27 GHz antenna array in a single laminate layout is proposed. Differently from the aforementioned works [24], [27], [28], the shared aperture antenna we propose aims to embed both the FR1, FR2 radiating systems on a single layer by using patch antennas for both the 5G frequency bands. We inserted the perfomance of our antennas is Table 2. The single-layer geometry allows, differently from the multilayer antennas presented in Tables 1, 2, an easy manufacturing, which overtakes the necessity of splitting the fabrication in different steps, and therefore the potential issues due to layers alignment and bonding [29]. The choice of a single-layer profile, suitable for the printed circuit board (PCB) manufacturing process, eases the antenna large-scale production and commercialization, even if usually drives

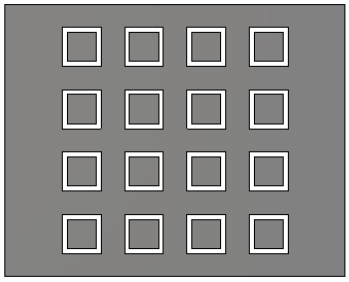

(a) Initial antenna design

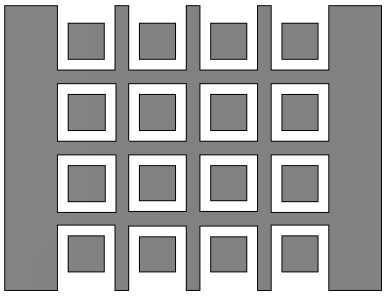

(b) Improved layout

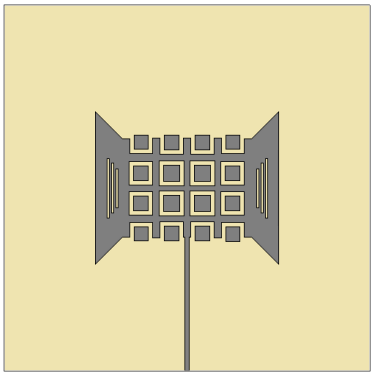

(c) Top view of the antenna final geometry

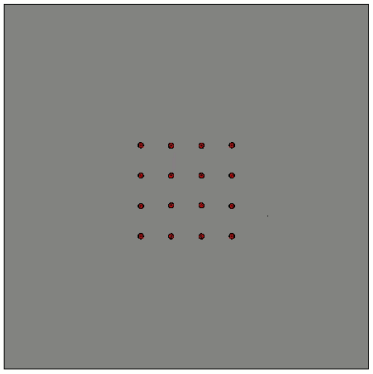

(d) Bottom view of the antenna final geometry (FR2 feeding system)

FIGURE 1. Shared aperture antenna.

and imposes constraints on the design [7]. Apart from the space saving, the FR2 array forces the FR1 antenna to a metallic patch shape which keeps the properties of low cross-polarization level.

The paper is organized as follows. First, in Section II the design of the shared-aperture antenna is described, here the considerations which lead the design to the final layout are explained. In section III the results for FR1 and FR2 frequency bands are presented and they are compared with the previously discussed state of art in section IV.

II. ANTENNA DESIGN

The two 5G bands operate at different wavelengths. Indeed, in free space the wavelength is 81.025 mm at 3.7 GHz, whereas it is 11.103 mm at 27 GHz, so that the ratio is around 7.36. This reflects on the characteristic dimensions of the antennas, and it makes the size of a 4×4 array in the mm-wave band comparable to a single patch in the lower band. For this reason, the two antenna layouts can be arranged together in the same area, by realizing a mm-wave patch array inside a grid slots etched in the lower band radiator. Hence, the low-band radiator has a grid-shape layout, whereas each element of the mm-wave array is surrounded by it. The coexistence of the two radiating systems in the same area affects both geometric parameters.

The antenna is tailored in PCB technology; a single 0.787 mm thick Rogers RT/duroid 5880 laminate ($\epsilon_r = 2.2$, $\tan\delta = 0.0004$) [30] hosts the whole shared aperture antenna, for an overall 0.857mm including the 35 μm metallizations. All the antennas are realized at the top metal level, which hosts the feeding network of the FR1 antenna, too, consisting of a microstrip line, whereas the bottom acts as ground for both the radiating systems. The top-view of an intuitive first layout for the antenna system is shown in Fig.1a. The larger metallization is the radiator operating at 3.7 GHz, whereas the small rectangles are associated to the 27 GHz array. The mm-wave patches are square, suitable also for dual polarization, and are fed via a set of coaxial cables inserted from the bottom (Fig. 1d). As it can be appreciated in the figures, the low-band antenna shape and its performances are strongly influenced by the mm-wave array. In addition, the FR1 antenna layout, due to the FR2 array insertion, forces the current resonant path and it can be exploited to improve the cross-polarization discrimination in the FR1 band. This leads to a modification in the antenna layout, by shaping the long sides close to the array. As shown in Fig. 1b, the metal segments of the FR1 patch close to the external lines on the mm-wave

array are removed. As a consequence, the different patches of the mm-wave array are affected by different coupling (i.e. the metallic surround rises the resonant frequency), so that different resonant sizes characterize the different elements. The cross-polarization discrimination is further improved by the insertion of two set slots in the radiator, parallel to the array (Fig. 1c), which help to improve the bandwidth. Finally, the FR1 radiator is shaped to achieve a bandwidth enlargement, and the final layout is shown in Fig. 1c, where the antenna lays on a 8×8 cm^2 large substrate. Moreover, the high mode resonances of the FR1 antenna must be considered to prevent that one of them falls inside the operative mm-wave frequency band; this could lead to undesired radiated fields fed by the coupling to the mm-wave array. [26], [31].

Another non-trivial issue is the definition of the feeding network. The geometry arrangement has to organize the two different feeding systems to avoid they overlap each other and minimize the interference between them. For this purpose, the FR1 patch is fed by a microstrip placed on the same metallization layer (Fig. 1c), by letting the bottom layer dedicated only to the mm-wave array feeding Fig. 1d). More precisely, the FR2 patches are fed via a set of 50 Ω coaxials (as displayed in Fig. 1d), Teflon(PTFE) filled ($\epsilon_r = 2.1$, $\tan_\delta = 0.0002$) and sized in order to have an internal conductor with a diameter equal to 0.3 mm.

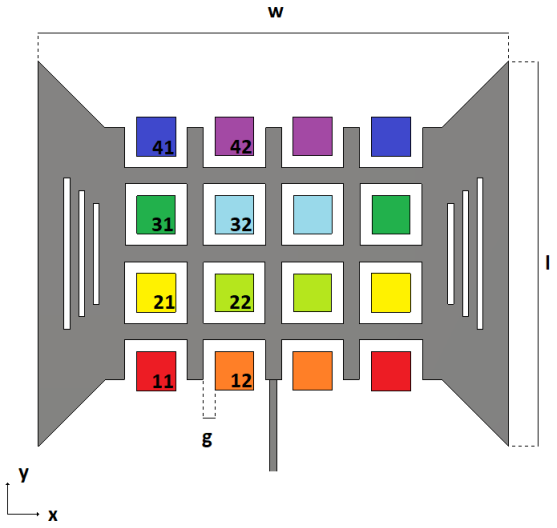

FIGURE 2. Top view of the antenna patches layout, the colors refer to the dimensions in Table 3.

As regards the FR2 antenna array, since the aforementioned different mutual couplings affect the operation, the patches will resonate at the same frequency for different lengths l. In addition, also the feeding point position with respect to the patch center, y_f, affects the antenna operation, leading to a different optimal size between, e.g., the patches in the upper and lower rows in the same horizontal position. By referring to Fig. 2, the patches highlighted with the same colors share the same size. In particular:

- the red-highlighted patches are surrounded by other array elements on 2 sides, and their feeding point offset is toward the array edge;
- the orange-highlighted patches are surrounded by other array elements on 3 sides, and their feeding point offset is toward the array edge;
- the yellow-highlighted patches are surrounded by other array elements on 3 sides, by the low-band patch on 1 side, and their feeding point offset is toward the array edge;
- the light green-highlighted patches are surrounded by other array elements on all the sides, and their feeding point offset is toward the array edge;
- the green-highlighted patches are surrounded by other array elements on 3 sides, by the low-band patch on 1 side, and their feeding point offset is toward the array center;
- the light blue-highlighted patches are surrounded by other array elements on all the sides, and their feeding point offset is toward the array center;
- the blue-highlighted patches are surrounded by other array elements on 2 sides, by the low-band patch on 1 side, and their feeding point offset is toward the array center;
- the violet-highlighted patches are surrounded by other array elements on 3 sides, and their feeding point offset is toward the array center;

These groups differ in terms of patch side and feed position. The geometric parameters of the array are listed in Table 3, in which the feed offset is intended parallel to the FR1 feeding microstrip. The spacing between the patch centres is 6.6 mm along both the x-y directions, equal to 0.6 λ_0 at 27 GHz. This spacing is enough to maintain a grid-shape in the FR1 antenna layout. As regards the FR1 antenna, its size is (l $\times$ w) = (33.06 $\times$ 39.5) mm^2, and a g = 1 mm gap is maintained around each mm-wave radiator. Two sets of three vertical slots are etched in the FR1 patch, alongside the array, centered in each of the lateral non interdigitated sections of the low-band radiator.

TABLE 3. Parameters of the FR2 array antenna: patch size l and feeding point offset with respect to the patch center y_f. Data are expressed in [mm].

Element	l	y_f
	3.27	0.85
	3.32	0.90
	3.27	0.90
	3.23	0.75
	3.24	0.80
	3.32	0.9
	3.28	0.9
	3.3	1.0

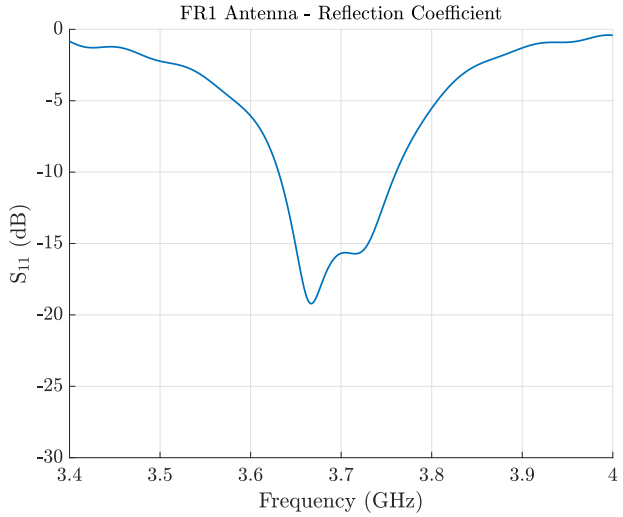

FIGURE 3. Reflection coefficient of the FR1 antenna.

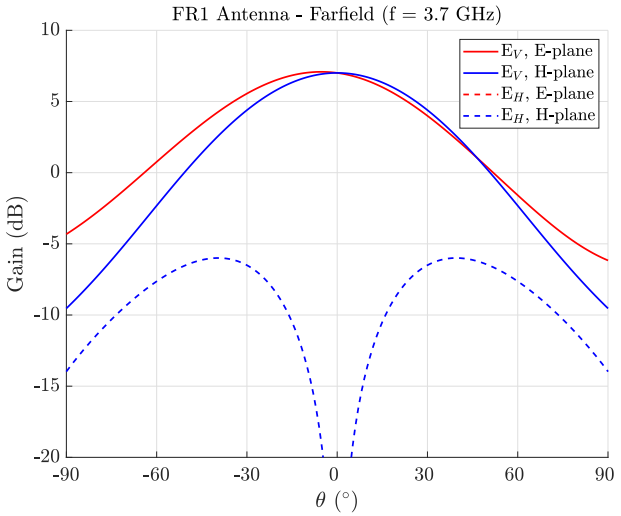

FIGURE 4. Gain pattern of the FR1 antenna.

III. RESULTS

The antenna system has been designed and simulated by using CST Microwave Studio. The performances have been evaluated in both the aforementioned frequency bands and are discussed in the following subsections. Since the antenna system is intended to work simultaneously at both FR1 and FR2 frequency bands, the 3dB-beamwidth at 3.7 GHz has been adopted to evaluate the beam steering properties of the mm-wave array, to guarantee an angular range where both the frequency bands are serviced. In the following results, the co-polar component of the electric field is the vertical one (E_v), whereas the cross-polar is the horizontal (E_H).

A. FR1 ANTENNA

The arrangement of the mm-wave array noticeably affects the path of the surface current within the FR1 band, impacting both the co-polar and the cross-polar components of the radiated fields. Consequently, despite the primary objective of the array layout being aperture reuse, specific details are adjusted to enhance the radiation pattern in the FR1 band.

The antenna is fed via a microstrip line, as in Fig. 1c. The scattering parameter $|S_{11}|$ is plotted in Fig. 3, which shows a 10-dB bandwidth of 130.4 MHz@3.69 GHz, equal to 3.5 in percentage terms. The gain of the co-polar component is 7.01 dB, with a 3-dB beamwidth of 69° in the E-plane and 62° in the H-plane, and a very high cross-polar component discrimination (see Fig. 4), which maintains a level higher than 20 dB at 30° in the H-plane, while also exhibiting excellent performance in the E-plane thanks to the layout symmetry.

B. FR2 ANTENNA ARRAY

The antenna has to serve the communication in the FR2 band inside a solid angle, in this case defined by the FR1 beamwidth. Because of this, it is important to evaluate how the scattering parameters, and therefore the operative 10dB BW of the whole array, are affected by the different phase distributions which provide the beam steering radiation [32], [33]. Thus, the FR2 array has been designed to satisfy the operational bandwidth over the whole solid angle covered by the its own beam steering, and its performance are evaluated in terms of active scattering parameters [32]. It is supposed an uniform excitation in terms of amplitude over the whole array, whereas the phase distributions are defined by the phase delays ϕ listed in Table 5, which indicate the difference in phase between the excitations of two consecutive array elements along the x-axis in Fig. 2. The resulting set of geometrical parameters which describes the array is listed in Table 3. In Fig. 5, the absolute amplitudes of the active scattering parameters relative to such distributions are displayed, which take into account the phase distribution over the feeding system and the coupling between the ports. The data relative to such results are listed in Table 4. They result in an overall 10dB bandwidth equal to 1.12 GHz @ 26.89 GHz kept along the whole steer angle domain, equal to a 4.15 in percentage terms. In the plot, the generic S-parameter $S_{ij,ij}$ refers to the patch element in the i-th row and j-th column in Fig. 1c, named {1,1} the element on the bottom left (see Fig. 2).

Because the array arrangement, and the presence of the conductor dedicated to low-band radiation, the far-field of the mm-wave elements are perturbed compared to the isolated

TABLE 4. Active 10dB frequency band of the FR2 array.

ϕ (deg.)	BW (GHz)	f_0 (GHz)	f_{c1} (GHz)	f_{c2} (GHz)
0	1.652	26.998	26.172	27.824
38	1.468	26.946	26.212	27.68
76	1.216	26.892	26.284	27.5
114	1.116	26.882	26.324	27.44

ϕ = Phase Delay, BW = 10dB Impedance Bandwidth,
f_0 = Array 10dB central frequency,
f_{c1} = Array minimum 10dB frequency,
f_{c2} = Array maximum 10dB frequency.

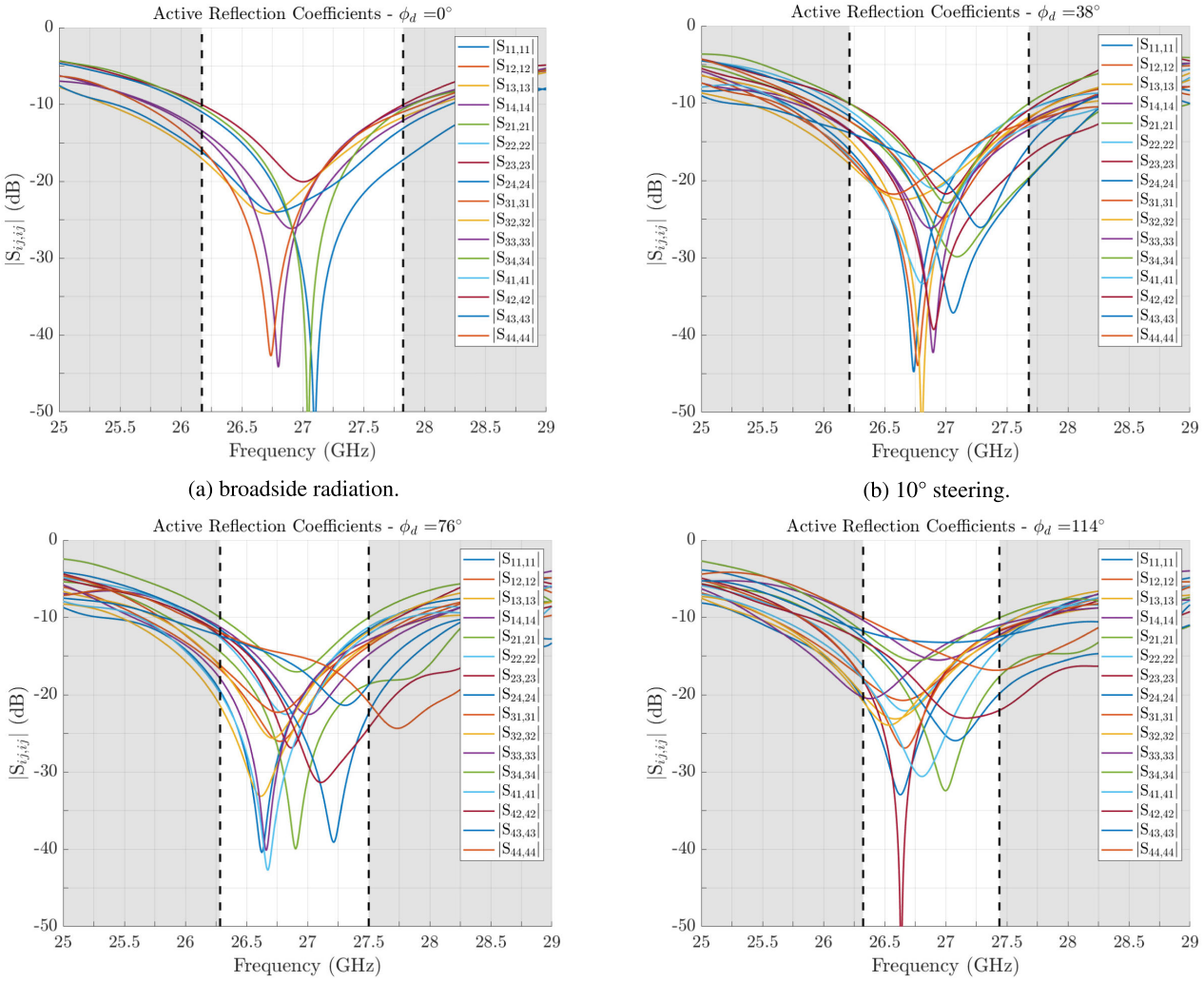

(a) broadside radiation.

(b) 10° steering.

(c) 20° steering.

(d) 30° steering.

FIGURE 5. Active S-Parameters of the FR2 array for the different phase distributions (and therefore beam steering angles) listed in Table 5. The grey patches highlight the 10dB frequency band in each considered steering angle.

elements. However, as depicted in Fig. 7, which illustrates the embedded gains of each array elements, the main lobe directions and cross-polarization values remain within acceptable limits for 5G applications. This is confirmed when the far-field of the entire mm-wave array is considered (Fig. 6). The gain is equal to 18.56 dB in the broadside direction. Named G_{co} the co-polar component of the gain, and G_{cross} the cross-polar one (respectively, E_V and E_H in Fig. 6), an important observation is that the cross polar discrimination (G_{co} - G_{cross}) maintains levels above 25 dB across the angular range [−45°, 45°] in the E-plane and remains above 60 dB in the H-plane (the cross-polar curve E_H on E-plane is not shown in Fig. 6). Additionally the cross-polar component is theoretically 134.38 dB lower than the co-polar component in the broadside.

Moreover, the far-field of the whole array is investigated at broadside and in terms of beam steering. In Fig. 6b the gain of the mm-wave array is displayed at the frequency of 27 GHz

TABLE 5. Beam steering performance of the FR2 array antenna (f=27 GHz).

ϕ [°]	MLD [°]	G [dB]	SLL [dB]
0	0	18.54	−13.99
38	10	18.30	−11.90
76	20	17.97	−11.00
114	30	17.36	−9.61
152	40	15.58	−3.93

ϕ = phase delay, MLD = Main Lobe Direction
G = Gain, SLL = Side Lobe Level

up to 40 degrees on beam steering in the H plane. In the graph, the solid lines are the co-polar components, the dotted are the cross-polar. The main data of the steering performance are listed in Table 5. It can be observed how the performance strongly degrades over 30° steering, mainly in terms of side lobe levels, nevertheless this angular range with downgraded perfomance is out of the FR1 main beam (which is 62° wide

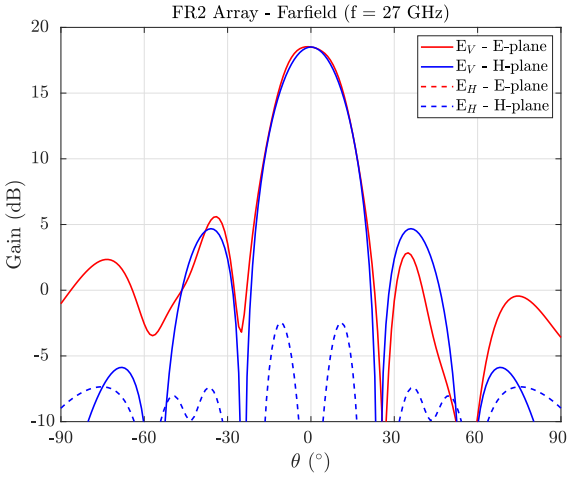

(a) Broadside radiation: co-polar (E_V, solid line) and cross-polar (E_H, dashed line) component along the E- and H- planes.

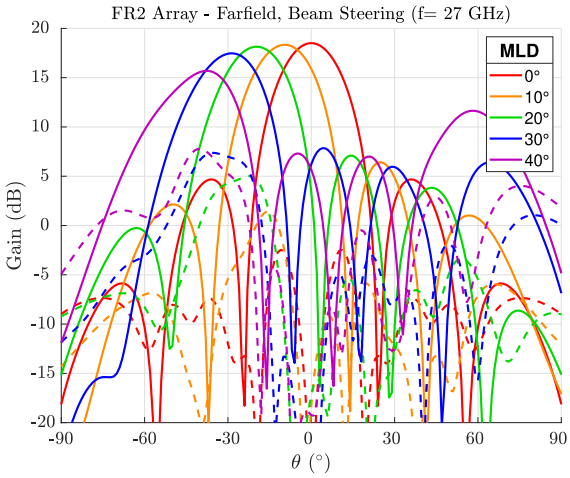

(b) Beam steering of the co-polar (solid line) and cross-polar (dashed) component along the H-plane. (MLD = Main Lobe Direction).

FIGURE 6. **Farfield performance of the FR2 array, radiation pattern of the gain at 27 GHz. The details are listed in Table 5.**

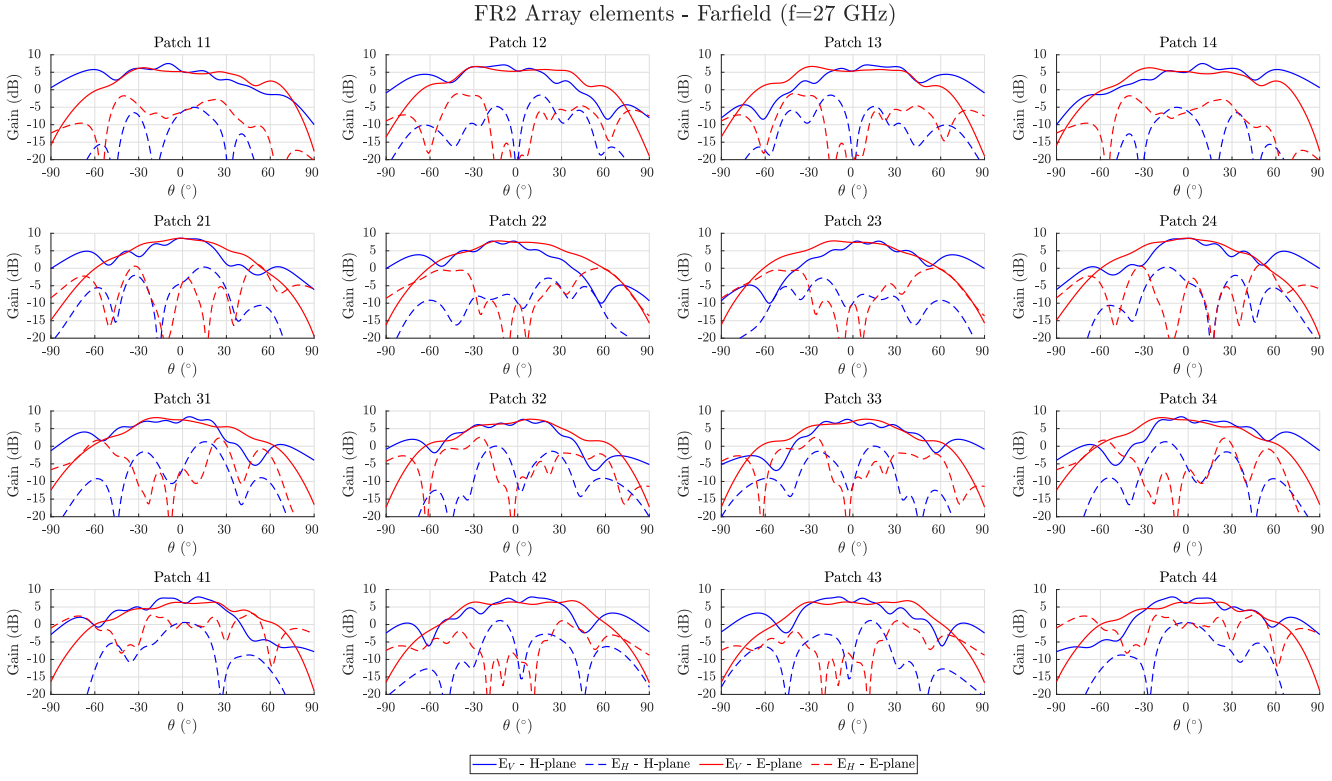

FIGURE 7. **Farfield of the FR2 array elements.**

on the H-plane, so it covers the [−31°:31°] angular aperture), so that it is not necessary to be covered by the beam steering in the FR2 frequency band.

IV. CONCLUSION

The antenna proposed in this work demonstrates how the relevant difference between the two FR1 and FR2 5G frequency bands allows incorporating both the radiating elements in the same antenna system, by implementing in the same laminate a 3.7 GHz antenna and a 27 GHz array. This can be obtained by a very simple layout, which does not require high costs and does not complicate the manufacturing process. The geometry provides a high cross-polar discrimination in the FR1 band.

Compared with the state of the art of Tables 1, 2, the antenna we propose is very low-profile. Antennas as [17], [18], [19], [20], [21], [22], [23], [25], [26] have larger overall profiles, up to 5-10 times, and, being multilayer [17], [18], [19], [20], [21], [25], [26] or characterized by a 3D metallic radiator [22], or by a reflector [23], they require a more complex manufacturing process. On the other side, the patch antennas do not provide a wide bandwidth, especially in the FR1 band, and our antenna is comparable to [21], [24], and [26] which, however, present multilayer geometries [21], [26], or thicker profiles [24]. The beam steering capability is similar to the aforementioned works [24], [26]. Therefore, we conclude that a very thin, simple and cheap layout does not affect sensibly the performance of the shared-aperture antenna, which keeps performance which are comparable with the state of the art. It is worth mentioning that, even if our proposed antenna is claimed to be single layer, the profile height equal to the Duroid laminate thickness (0.857 mm considering a 35μm metal thickness) does not take into account of the FR2 feeding network, which consists of a set of coaxials. Anyway, if this was replaced by a microstrip network, which implies a Prepreg layer and another Rogers RT/duroid RT5880 laminate (e.g. 0.252mm or 0.508 mm thick), this would lead to a total thickness less than 1.5 millimeters, so keeping a very low profile shared aperture antenna. From a performance point of view, the antenna provides respectively a 3.5% and 4.17% percentage bandwidth in the FR1 and FR2 bands. However, the works on low-profile antennas for 5G with a beam steering capability summarized in Table 2 [24], [25], [26], [27], [28] do not provide the operative bandwidth in terms of active S-parameters to perform a direct comparison.

It is worth noting that the FR2 beam steering capability, as, mainly, the angular range, could be improved by approaching the array elements, but this requires a deep modification of the layout, also in terms of stack up. Indeed, if we approach the patches keeping their size similar to the ones presented in the paper, the necessity of a gap between the metalizations makes the metal grid, which forms the FR1 patch, disappear. Therefore, the design of a $0.5\lambda_0$ spaced array would require further solutions to miniaturize the patches. The easiest way is to add a dielectric superstrate over the radiating layer. This further layer would help also in bandwidth enlargement, at the cost of an increase in the antenna profile.

REFERENCES

[1] J. Nightingale, P. Salva-Garcia, J. M. A. Calero, and Q. Wang, "5G-QoE: QoE modelling for ultra-HD video streaming in 5G networks," *IEEE Trans. Broadcast.*, vol. 64, no. 2, pp. 621–634, Jun. 2018, doi: 10.1109/TBC.2018.2816786.

[2] L. Chettri and R. Bera, "A comprehensive survey on Internet of Things (IoT) toward 5G wireless systems," *IEEE Internet Things J.*, vol. 7, no. 1, pp. 16–32, Jan. 2020, doi: 10.1109/JIOT.2019.2948888.

[3] A. Acemoglu, J. Krieglstein, D. G. Caldwell, F. Mora, L. Guastini, M. Trimarchi, A. Vinciguerra, A. L. C. Carobbio, J. Hysenbelli, M. Delsanto, O. Barboni, S. Baggioni, G. Peretti, and L. S. Mattos, "5G robotic telesurgery: Remote transoral laser microsurgeries on a cadaver," *IEEE Trans. Med. Robot. Bionics*, vol. 2, no. 4, pp. 511–518, Nov. 2020, doi: 10.1109/TMRB.2020.3033007.

[4] E. Kampert, C. Schettler, R. Woodman, P. A. Jennings, and M. D. Higgins, "Millimeter-wave communication for a last-mile autonomous transport vehicle," *IEEE Access*, vol. 8, pp. 8386–8392, 2020, doi: 10.1109/ACCESS.2020.2965003.

[5] (2022). *WRC-23 Booklet: Agenda and Relevant Resolutions*. [Online]. Available: https://www.itu.int/hub/publication/r-act-arr-1-2022/

[6] *GSMA—5G mmWave Deployment Best Practices Whitepaper*. Accessed: May 2024. [Online]. Available: https://www.gsma.com/solutions-and-impact/technologies/networks/gsma_resources/5g-mmwave-deployment-best-practices-whitepaper/

[7] M. Simone, S. C. Pavone, M. B. Lodi, N. Curreli, G. Muntoni, A. Fanti, G. Sorbello, and G. Mazzarella, "Design of a low-profile dual linearly polarized antenna array for mm-wave 5G," *IEEE Access*, vol. 11, pp. 40645–40656, 2023, doi: 10.1109/ACCESS.2023.3268029.

[8] J. F. Zhang, Y. J. Cheng, and Y. R. Ding, "An S- and V-band dual-polarized antenna based on dual-degenerate-mode feeder for large frequency ratio shared-aperture wireless applications," *IEEE Trans. Antennas Propag.*, vol. 68, no. 12, pp. 8127–8132, Dec. 2020, doi: 10.1109/TAP.2020.2983769.

[9] D. E. Serup, G. F. Pedersen, and S. Zhang, "Dual-band shared aperture reflectarray and patch antenna array for S- and Ka-bands," *IEEE Trans. Antennas Propag.*, vol. 70, no. 3, pp. 2340–2345, Mar. 2022, doi: 10.1109/TAP.2021.3111171.

[10] S. Liu, K. Jiang, G. Xu, X. Ding, K. Zhang, J. Fu, and Q. Wu, "A dual-band shared aperture antenna array in Ku/Ka-bands for beam scanning applications," *IEEE Access*, vol. 7, pp. 78794–78802, 2019, doi: 10.1109/ACCESS.2019.2922647.

[11] Y. Lu, Y. You, Q. You, Y. Wang, and J. Huang, "Dual-band shared-aperture variable inclination continuous transverse stub antenna," *IEEE Trans. Antennas Propag.*, vol. 71, no. 1, pp. 463–472, Jan. 2023, doi: 10.1109/TAP.2022.3212043.

[12] L. Kong and X. Xu, "A compact dual-band dual-polarized microstrip antenna array for MIMO-SAR applications," *IEEE Trans. Antennas Propag.*, vol. 66, no. 5, pp. 2374–2381, May 2018, doi: 10.1109/TAP.2018.2814222.

[13] J. Ran, Y. Wu, C. Jin, P. Zhang, and W. Wang, "Dual-band multipolarized aperture-shared antenna array for Ku-/Ka-Band satellite communication," *IEEE Trans. Antennas Propag.*, vol. 71, no. 5, pp. 3882–3893, May 2023, doi: 10.1109/TAP.2023.3248445.

[14] Y. Asci, "Wideband and stable-gain cavity-backed slot antenna with inner cavity walls and baffle for X- and Ku-band applications," *IEEE Trans. Antennas Propag.*, vol. 71, no. 4, pp. 3689–3694, Apr. 2023, doi: 10.1109/TAP.2023.3239168.

[15] M. Ferrando-Rocher, J. I. Herranz-Herruzo, A. Valero-Nogueira, and B. Bernardo-Clemente, "Full-metal K-Ka dual-band shared-aperture array antenna fed by combined ridge-groove gap waveguide," *IEEE Antennas Wireless Propag. Lett.*, vol. 18, pp. 1463–1467, 2019, doi: 10.1109/LAWP.2019.2919928.

[16] Y. Yao, X. Q. Lin, T. Qin, Y. Su, and X. Yang, "Shared-aperture Ka-band reflectarray and X-band phased array for broadband inter-satellite communication," *IEEE Trans. Antennas Propag.*, vol. 70, no. 11, pp. 11199–11204, Nov. 2022, doi: 10.1109/TAP.2022.3209249.

[17] T. H. Brandão and A. Cerqueira S., "Triband antenna array for FR1/FR2 5G NR base stations," *IEEE Antennas Wireless Propag. Lett.*, vol. 22, pp. 764–768, 2023, doi: 10.1109/LAWP.2022.3224827.

[18] Y. Cheng and Y. Dong, "Dual-broadband dual-polarized shared-aperture magnetoelectric dipole antenna for 5G applications," *IEEE Trans. Antennas Propag.*, vol. 69, no. 11, pp. 7918–7923, Nov. 2021, doi: 10.1109/TAP.2021.3083744.

[19] G. Yang and S. Zhang, "Dual-band shared-aperture multiple antenna system with beam steering for 5G applications," *IEEE Trans. Circuits Syst. II, Exp. Briefs*, vol. 69, no. 12, pp. 4804–4808, Dec. 2022, doi: 10.1109/TCSII.2022.3201009.

[20] T. Li and Z. N. Chen, "Shared-surface dual-band antenna for 5G applications," *IEEE Trans. Antennas Propag.*, vol. 68, no. 2, pp. 1128–1133, Feb. 2020, doi: 10.1109/TAP.2019.2938584.

[21] L. Wen, T. Ji, Y. Huang, T. Cao, Z. Yu, C. Chen, L. Zhu, J. Zhou, and W. Hong, "A dual-polarized aperture-sharing phased-array antenna for 5G (3.5, 26) GHz communication," *IEEE Trans. Antennas Propag.*, vol. 71, no. 5, pp. 3785–3796, May 2023, doi: 10.1109/TAP.2023.3245183.
[22] J. N. Hao, L. Y. Feng, W. S. Ji, and Y. Liu, "Dual-wideband dual-frequency antenna with large frequency ratio for 5G applications," *IEEE Trans. Antennas Propag.*, vol. 72, no. 2, pp. 1887–1892, Feb. 2024, doi: 10.1109/tap.2023.3333539.
[23] J. Wu, C. Wang, and Y. X. Guo, "A compact reflector antenna fed by a composite S/Ka-band feed for 5G wireless communications," *IEEE Trans. Antennas Propag.*, vol. 68, no. 12, pp. 7813–7821, Dec. 2020, doi: 10.1109/TAP.2020.3000858.
[24] R. S. Malfajani, F. B. Ashraf, and M. S. Sharawi, "A 5G enabled shared-aperture, dual-band, in-rim antenna system for wireless handsets," *IEEE Open J. Antennas Propag.*, vol. 3, pp. 1013–1024, Aug. 2022. [Online]. Available: https://ieeexplore.ieee.org/document/9868831, doi: 10.1109/OJAP.2022.3201627.
[25] Q. Liang, H. Aliakbari, and B. K. Lau, "Co-designed millimeter-wave and sub-6 GHz antenna for 5G smartphones," *IEEE Antennas Wireless Propag. Lett.*, vol. 21, pp. 1995–1999, 2022, doi: 10.1109/LAWP.2022.3187782.
[26] X.-H. Ding, W.-W. Yang, H. Tang, L. Guo, and J.-X. Chen, "A dual-band shared-aperture antenna for microwave and millimeter-wave applications in 5G wireless communication," *IEEE Trans. Antennas Propag.*, vol. 70, no. 12, pp. 12299–12304, Dec. 2022, doi: 10.1109/TAP.2022.3209220.
[27] M. Ikram, N. Nguyen-Trong, and A. M. Abbosh, "Common-aperture sub-6 GHz and millimeter-wave 5G antenna system," *IEEE Access*, vol. 8, pp. 199415–199423, 2020, doi: 10.1109/ACCESS.2020.3034887.
[28] C. Wang, W. Cao, W. Ma, C. Li, and J. Jing, "Dual-band structure reused aperture-sharing antenna with low sidelobe and high gain for 5G communication," *IEEE Antennas Wireless Propag. Lett.*, vol. 23, pp. 1386–1390, 2024, doi: 10.1109/lawp.2024.3356614.
[29] T. Potelon, M. Ettorre, L. Le Coq, T. Bateman, J. Francey, and R. Sauleau, "Reconfigurable CTS antenna fully integrated in PCB technology for 5G backhaul applications," *IEEE Trans. Antennas Propag.*, vol. 67, no. 6, pp. 3609–3618, Jun. 2019, doi: 10.1109/TAP.2019.2902644.
[30] *RT/Duroid Registered 5880 Laminates*. Accessed: May 2024. [Online]. Available: https://www.rogerscorp.com/advanced-electronics-solutions/rt-duroid-laminates/rt-duroid-5880-laminates
[31] Y. Liu, Y. Li, L. Ge, J. Wang, and B. Ai, "A compact hepta-band mode-composite antenna for sub (6, 28, and 38) GHz applications," *IEEE Trans. Antennas Propag.*, vol. 68, no. 4, pp. 2593–2602, Apr. 2020, doi: 10.1109/TAP.2019.2955206.
[32] D. M. Pozar, "The active element pattern," *IEEE Trans. Antennas Propag.*, vol. 42, no. 8, pp. 1176–1178, Aug. 1994, doi: 10.1109/8.310010.
[33] D. M. Pozar, "A relation between the active input impedance and the active element pattern of a phased array," *IEEE Trans. Antennas Propag.*, vol. 51, no. 9, pp. 2486–2489, Sep. 2003, doi: 10.1109/tap.2003.816302.

MARCO SIMONE (Member, IEEE) received the master's degree in electronic engineering and the Ph.D. degree in electronic and computer engineering from the University of Cagliari, Italy, in 2011 and 2016, respectively. He was a Visiting Ph.D. Student with the Queen Mary University of London (QMUL), London, U.K., in 2015, where he was also a Postdoctoral Research Assistant with the Antennas & Electromagnetics Research Group, in 2016 and 2017. From 2017 to 2022, he was an Associate Researcher with the Laboratory of Applied Electromagnetics, University of Cagliari, where he has been an Assistant Professor in electromagnetic fields, since 2023. His research interests include optimization techniques applied to electromagnetics problems, microwave components design for radioastronomy applications, antennas design for 5G, satellite, and mm-wave applications.

SANTI CONCETTO PAVONE (Senior Member, IEEE) received the B.Sc. and M.Sc. degrees (cum laude) in electronics engineering from the University of Messina, Italy, in 2010 and 2012, respectively, and the Ph.D. (Doctor Europaeus) degree in information engineering and science (research line: electromagnetics engineering) from the University of Siena, Italy, in 2015. He was a Visiting Ph.D. Student and a Visiting Assistant Professor with the Institut d'Èlectronique et de Télécommunications de Rennes (IETR), Rennes, France, in 2015 and 2020, respectively. From July 2016 to July 2019, he was an Associate Researcher with the Laboratory of Applied Electromagnetics, University of Siena. Since August 2019, he has been an Assistant Professor with the Department of Electrical, Electronics, and Information Engineering, University of Catania, Italy. His current research interests include electromagnetic theory, scattering theory, RADAR design at millimeter waves, high-frequency techniques, focusing systems, non-diffractive localized pulses, and reconfigurable antennas. He was a recipient of the ESF Research Networking Programme "NEWFOCUS" Scholarship, in 2015, and the IEEE AP-S Student Award granted by the AP-S/MTT-S Chapter Central-Southern Italy, in 2014. In 2017, he was a Finalist of the Best Paper Award in Electromagnetics and Antenna Theory at the 11th European Conference on Antennas and Propagation (EuCAP), Paris. In 2018, he was a co-recipient of the Best Paper Award in Electromagnetics and Antenna Theory at the 12th EuCAP, London. In 2020, he got Italian Scientific Habilitation for Associate Professorship of Electromagnetic Fields. In 2020, 2021, and 2022, he was selected among outstanding reviewers of IEEE Transactions on Antennas and Propagation. In 2019, 2021, and 2022, he was a recipient of Young Scientist Awards at the 41st Progress in Electromagnetics Research Symposium (Rome), at the XXXIV General Assembly and Scientific Symposium of the International Union of Radio Science (Rome), and at the Third Atlantic Asia–Pacific Radio Science Meeting (Gran Canaria, Spain). He serves as an Associate Editor for IEEE Access, *IET Electronics Letters*, and *Frontiers in Antennas and Propagation*.

MATTEO BRUNO LODI (Member, IEEE) received the bachelor's degree in biomedical engineering from the University of Cagliari, Cagliari, in 2016, and the master's degree in biomedical engineering from the Politecnico di Torino, Turin, Italy, in 2018. He is currently pursuing the Ph.D. degree in electronic engineering and computer science with the University of Cagliari. His research interests include the modeling of bioelectromagnetic phenomena, especially hyperthermia treatment, the study, manufacturing, synthesis of magnetic biomaterials for tissue engineering applications, and the use of microwave for biotechnology and environmental applications. He was awarded as the Young Scientists at General Assembly and Scientific Symposium of URSI, in 2020 and 2021. He has been appointed as a Representative of the Young Professionals of IEEE Region 8 Nanotechnology Council. He is a member of the Editorial Board of the IEEE Future Directions Technology Policy and Ethics Newsletter.

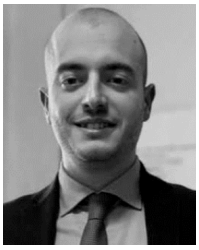

NICOLA CURRELI (Member, IEEE) received the M.Sc. degree from the University of Genoa, Genoa, Italy, in 2016, and the joint Ph.D. degree in electronic engineering from the University of Cagliari, Cagliari, Italy, and Italian Institute of Technology (IIT), Genoa, in 2020. After completing the Ph.D. degree, he held a fellow with Graphene Laboratories, IIT, within the Graphene Core 2 Project (Graphene Flagship). In 2019, he was a Visiting Researcher with the Physics and Mechanical Engineering Departments, Columbia University, New York City, NY, USA, as part of the Marie Sklodowska-Curie SONAR H2020 Action. Between 2022 and 2023, he was a Visiting Researcher with the Molecular Foundry, Lawrence Berkeley National Laboratory, Berkeley, CA, USA. He is currently a Postdoctoral Researcher with the Functional Nanosystems Group, IIT. His research interests include the study of low-dimensional materials, their characterization and their application in the field of photonics, the design, implementation, analysis of linear and nonlinear integrated optical, microwave devices, and antennas. He is a member of the Topical Advisory Panel of Photonics. He was a recipient of the Young Scientists at the General Assembly and Scientific Symposium of URSI, in 2022.

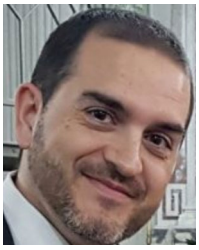

GIACOMO MUNTONI (Member, IEEE) received the Graduate degrees in electronic engineering and telecommunication engineering and the Ph.D. degree in electronic engineering and computer science from the University of Cagliari, in 2010, 2015, and 2019, respectively. He is currently a Technologist with the Applied Electromagnetics Group, University of Cagliari. His research interests include design and characterization of antennas for biomedical and aerospace applications, microwave-based dielectric characterization of materials, 3-D printing of RF components, and monitoring of the space debris environment in low earth orbit with the Sardinia radio telescope, in collaboration with Cagliari Astronomical Observatory.

ALESSANDRO FANTI (Senior Member, IEEE) received the Laurea degree in electronic engineering and the Ph.D. degree in electronic engineering and computer science from the University of Cagliari, Cagliari, Italy, in 2006 and 2012, respectively. From 2013 to 2016, he was a Postdoctoral Fellow of the Electromagnetic Group, University of Cagliari, where he was an Assistant Professor in electromagnetic fields with the Department of Electrical and Electronic Engineering, from March 2017 to March 2024. He is currently an Associate Professor with the University of Cagliari. He has authored or coauthored 67 articles in international journals. His research interests include the use of numerical techniques for modes computation of guiding structures, optimization techniques, analysis and design of waveguide slot arrays, analysis and design of patch antennas, radio propagation in urban environment, modeling of bioelectromagnetic phenomena, and microwave exposure systems for biotechnology and bioagriculture. He is a member of the IEEE Antennas and Propagation Society, Italian Society of Electromagnetism, National Inter-University Consortium for Telecommunications, and Interuniversity Center for the Interaction Between Electromagnetic Fields and Biosystems. From 2020 to 2023, he had been acting as a Principal Investigator of the IAPC Project, which was funded with five million euros by Italian Ministry of Economic Development (MISE), within the AGRIFOOD PON I&C (2014–2020). Since 2024, he has been acting as a Principal Investigator of the AISAC Project funded with 15 million euros by Italian Ministry of Enterprises and Made in Italy (MIMIT), within the "ACCORDI PER L'INNOVAZIONE" (2021–2026). He is an Associate Editor of the IEEE JOURNAL OF ELECTROMAGNETICS, RF AND MICROWAVES IN MEDICINE AND BIOLOGY.

GINO SORBELLO (Member, IEEE) received the Laurea degree (cum laude) in electronics engineering from the University of Catania, Catania, Italy, in 1996, and the Ph.D. degree in electronics and communications engineering from the Polytechnic Institute of Milan, Milan, Italy, in 2000. He became an Assistant Professor in electromagnetic fields with the University of Catania, in 2002, where he has been an Associate Professor in electromagnetic fields with the Department of Electrical, Electronics, and Computer Engineering, since 2014. Since 2012, he has been a member of INFN-LNS and collaborates with the Ion Sources and Plasma Physics Group. His current research interests include single-mode solid-state waveguide lasers and amplifiers, integrated optics, development of planar antennas and ultra-wideband compact antennas, and the study of microwave devices and computational electromagnetism, with a special interest in RF-plasma interactions and particle accelerators.

GIUSEPPE MAZZARELLA (Senior Member, IEEE) received the Graduate degree (summa cum laude) in electronic engineering from the Università Federico II of Naples, in 1984, and the Ph.D. degree in electronic engineering and computer science, in 1989. In 1990, he became an Assistant Professor with the Dipartimento di Ingegneria Elettronica, Università Federico II of Naples. Since 1992, he has been with the Dipartimento di Ingegneria Elettrica ed Elettronica, Università di Cagliari, as an Associate Professor and then, since 2000, as a Full Professor, teaching courses in electromagnetics, microwave, antennas, and remote sensing. His research interests include efficient design of large arrays of slots and power synthesis of array factor, with emphasis on inclusion of constraints, microwave holography techniques for the diagnosis of large reflector antennas, use of evolutionary programming for the solution of inverse problems, in particular problems of synthesis of antennas, and periodic structures. He is the author (or coauthor) of over 100 articles in international journals and is a reviewer of many EM journals.

Open Access funding provided by 'Università degli Studi di Cagliari' within the CRUI CARE Agreement